INSTITUTE OF PHYSICS PUBLISHING JOURNAL OF PHYSICS B: ATOMIC, MOLECULAR AND OPTICAL PHYSICS

J. Phys. B: At. Mol. Opt. Phys. **35** (2002) 3829–3845 PII: S0953-4075(02)36904-9

Electron impact ionization of argon ions (q = 4–11)

H Zhang, S Cherkani-Hassani, C Bélenger, M Duponchelle, M Khouilid[1], E M Oualim[2] and P Defrance[3]

Catholic University of Louvain, Department of Physics, Chemin du Cyclotron 2, B-1348 Louvain-la-Neuve, Belgium

E-mail: defrance@fyam.ucl.ac.be

Received 13 May 2002, in final form 16 July 2002
Published 2 September 2002
Online at stacks.iop.org/JPhysB/35/3829

Abstract

Absolute cross sections for electron impact ionization of multiply charged argon ions (Ar^{q+}) have been measured in an animated crossed electron–ion beam experiment. Results are reported for single ionization (SI) (q = 4–6, 8, 10 and 11) ions and for double ionization (DI) (q = 5–11). The measurements cover the energy range from threshold to about 6000 eV. The direct process is seen to dominate SI for q = 8, 10 and 11. For charge states 4–6, excitation–autoionization processes are seen to largely contribute to the ionization signal. In addition, metastable states are unambiguously identified for Ar^{5+} and Ar^{6+}. Ionization–autoionization (IA) from the L shell accounts predominantly for DI of Ar^{q+} (q = 5, 6). For charge states 7–11 direct DI is found to decrease strongly with respect to IA from the K shell.

1. Introduction

Among rare gases, argon is of standard use for fusion plasma diagnostics (Janev 1993). Subsequently, plasma modelling requires a good understanding of electron impact single ionization (SI) for multiply charged argon ions. In addition, investigations of double ionization (DI) processes add to the global knowledge of electron impact ionization. In the present paper, we report on electron impact cross section measurements for SI of Ar^{q+} (q = 4–6, 8, 10 and 11) and for DI of Ar^{q+} (q = 5–11), from below the respective threshold to a maximum energy of 6000 eV. Some of the reactions under investigation here have already been subject to experimental studies: SI for q = 4–6 and 8 and DI for q = 5–7. Those works were performed in our laboratory (Louvain-la-Neuve) or in the laboratories of Giessen and Oak Ridge and the corresponding references are given in section 3. The present series of absolute total cross section

[1] Present address: Université Chouaib-Doukkali, Faculté des Sciences, km 1, Route Ben Maachou, BP 20, El Jadida, Morocco.

[2] Present address: Université Hassan 1er, Faculté des Sciences et Techniques, BP 577, Route de Casablanca, Settat, Morocco.

[3] Author to whom any correspondence should be addressed.

0953-4075/02/183829+17$30.00

results extends the energy range covered by previous experiments and the improved precision of the data allows a detailed analysis of the respective role of direct and indirect processes in the present cases. Particular attention is devoted to the identification of metastable states present in the primary beam and to their role both for SI and for DI.

From the theoretical point of view, electron impact direct SI of atoms and ions is usually described with a good accuracy by the distorted-wave Coulomb–Born approximation with exchange (DWBX). Results are available in that approximation for charge states 4–6 and 8. More refined approximations also include indirect processes. For Ar^{6+} (both in the ground and in the metastable state) calculations in the average-configuration distorted-wave approximation (ACDW) have been made by Pindzola *et al* (1986). The distorted-wave *R*-matrix method was also applied for Ar^{9+} (Laghdas *et al* 1995). For other ions, only predictions from semi-empirical formulae are available. Most of them may give satisfactory results in cases where indirect processes do not play a significant role.

For direct double ionization (DDI), theoretical results based on the Born approximation are presently available for direct ionization of helium-like ions only (Defrance *et al* 2000). In that calculation, shake-off is supposed to be dominant over two-step processes which are neglected, this approximation being supposed to be valid at high energy. The results show that the DDI cross section strongly reduces with increasing ion charge along the isoelectronic sequence. A similar reduction was observed in different experiments for members of other isoelectronic sequences and, in extreme cases, DI reactions are dominated by indirect processes, the main one being inner-shell ionization followed by autoionization (IA). This particular process is basically an SI process, which is usually much weaker than SI involving outer-shell electrons. As a consequence, it is not taken into account in the calculations and no theoretical results are presently available for comparison. However, a satisfactory estimate of its importance can be given by making use of a semi-empirical formula for inner-shell SI, for instance, the Lotz formula (1968) or the Deutsch–Märk formalism (Deutsch *et al* 2002). Next, the branching ratio for autoionization must be taken into account in order to estimate the contribution of IA to DI. Again, radiative and autoionization rates are not yet available for many ionic systems and, in these situations, because radiative decay of the resulting hollow multiply charged ion is negligible, the branching ratio is supposed to be unity in favour of autoionization.

2. Method and apparatus

In this experiment, the animated crossed beams method has been employed. The apparatus has essentially been described earlier (Duponchelle *et al* 1995). Argon ions are extracted from an ECR source (Barué *et al* 1989). Ions are accelerated by a voltage of 10 kV, mass-analysed and focused to the collision region. A magnetic mass analyser separates the product ions from the primary beam. Product ions are transmitted via a spherical deflector to a channeltron detector, while the primary ions are collected by a Faraday cup. A ribbon electron beam is produced in a Pierce cathode–anode configuration. As required by the animated beam method, the electron beam is swept mechanically across the ion beam in a seesaw motion. The ionization cross section is related to the measured quantities in the following way (Duponchelle *et al* 1995):

$$\sigma = \frac{H}{n} \underbrace{\frac{q e^2 v_e v_i}{\sqrt{v_e^2 + v_i^2}}}_{A} \sum_{j=1}^{n} \frac{k(j)}{\Delta t(j) i_i(j) i_e(j)} \tag{1}$$

where $k(j)$ is the number of events produced at position j of the sweeping motion for one passage of the electrons across the ion beam, $\Delta t(j)$ is the time spent at this position, A is the

kinematic parameter and v_e and v_i, e and qe and $i_e(j)$ and $i_i(j)$ are the velocities, charges and currents of the electrons and of the ions, respectively. H is the total vertical displacement of the electron beam and n is the number of steps. The electron and ion currents are frequency-converted and recorded according to the electron beam position in a multichannel analyser triggered by the signal showing the position of the encoder. Similar recordings are performed for the amplified detector pulses and for the pulses produced by the internal clock of the computer. The detector efficiency has been estimated to be 100% and a total transmission of ions from the collision to the detector has been established.

It is not possible to separate ions having nearly identical charge to mass ratio. This situation holds for the Ar^{5+} and Ar^{10+} primary ion beams, which are seen to contain O^{2+} and O^{4+} ions respectively, so that the true primary ion current is overestimated in the experiment. Absolute cross section measurement requires the determination of the impurity ion population. For this purpose, the following procedure was adopted: the analysing magnetic field is adjusted in order to collect separately the low intensity ion beams (Ar^{4+} and O^{+} or Ar^{9+} and O^{3+}) produced by the corresponding primary ions capturing an electron from residual gas molecules. The measured currents are proportional to the parent ion population and to the respective capture cross sections which are well known (Bliman *et al* 1983). The comparison of the measured currents with the primary ion beam intensity allows the relative impurity ion populations to be determined. Subsequently, the true primary ion current intensity is estimated with a satisfactory precision. In addition, the ionization products resulting from interaction of electrons with the impurities are separated from the true ion signal by the analysing magnetic field. The measured ion current ranges from 100 to 600 nA, depending on the source conditions for the different charge states, and the associated systematic and statistical errors are 0.5 and 1%, respectively. Table 1 gives typical working conditions for the reactions under investigation here.

The electron energy is corrected for contact potential (−0.5 eV) and the kinetic energy of ions is taken into account to obtain the absolute collision energy. The uncertainty on this energy is ±0.5 eV.

3. Results and discussion

The ionization and excitation energies relevant to the discussion of present results are extracted from data calculated by Clementi and Roetti (1974) and from the tables of Bashkin and Stoner (1975). They are presented in table 2 together with the thresholds observed in this experiment for SI and DI and for indirect processes, excitation–autoionization (EA) and IA. Results of cross section measurements together with electron energy are listed in tables 3 (SI, $q = 4$–6), 4 (SI, $q = 8$–11), 5 (DI, $q = 5$–6) and 6 (DI, $q = 7$ and 8–11). Errors represent one standard deviation of the counting statistics.

3.1. Single ionization

3.1.1. Ar^{4+}. Results are shown in figure 1 together with the experimental data of Donets and Ovsyannikov (1981) and Müller *et al* (1980) and the theoretical results of Younger (1981) based upon the distorted-wave exchange approximation (DWBX) for direct ionization only. Particular attention was paid to the low energy range because the experimental conditions were very favourable in this case (the signal over background ratio was large). So, the Ar^{4+} ground state, $[Ne]3s^2 3p^2\ ^3P$ ionization threshold was clearly observed at 75.1 eV and the contact potential (−0.5 eV) was precisely determined from this measurement. We note the satisfactory agreement between experimental data over the common energy range. The experimental data of Crandall *et al* (1979)—not shown in the figure—are slightly above present data and show

Table 1. Typical working conditions.

Parameter	Typical value	Error (%)	
		Systematic	Statistical
Kinematic factor		0.5	—
Velocity, u(mm s^{-1})	0.48	0.1	—
Electron current (I_e)	7–17 mA	0.5	1.0
	Counts (K); luminosity, L (10^{19} Hz cm^{-2})		
Ar^{4+} (SI)	68 600/33	1.0	0.2
Ar^{5+} (SI)	7800/7	1.0	0.1
Ar^{6+} (SI)	23 600/41	1.0	0.2
Ar^{8+} (SI)	9325/33	1.0	2.2
Ar^{10+} (SI)	360/0.6	1.0	6.2
Ar^{11+} (SI)	1570/4	1.0	6.1
Ar^{5+} (DI)	1600/25	1.0	1.8
Ar^{6+} (DI)	6200/46	1.0	2.0
Ar^{7+} (DI)	63/5.0	1.0	4.8
Ar^{8+} (DI)	31/6.0	1.0	4.2
Ar^{9+} (DI)	6/1.6	1.0	11.1
Ar^{10+} (DI)	5/1.0	1.0	9.1
Ar^{11+} (DI)	4/1.0	1.0	16.7
	Cross section, σ (10^{-19} cm^2)		
Ar^{4+} (SI)	84.3	2.6	2.2
Ar^{5+} (SI)	79.3	2.6	2.1
Ar^{6+} (SI)	37.8	2.6	2.2
Ar^{8+} (SI)	8.07	2.6	4.2
Ar^{10+} (SI)	3.23	2.6	8.2
Ar^{11+} (SI)	2.29	2.6	8.1
Ar^{5+} (DI)	11.6	2.6	3.8
Ar^{6+} (DI)	7.67	2.6	4.0
Ar^{7+} (DI)	0.21	2.6	6.8
Ar^{8+} (DI)	0.048	2.6	6.2
Ar^{9+} (DI)	0.027	2.6	13.1
Ar^{10+} (DI)	0.022	2.6	11.1
Ar^{11+} (DI)	0.018	2.6	18.7

a bump around 300 eV, which was not reproduced, either here or by Müller's experiment. EA is observed only in the low energy range: just above the threshold, the cross section is seen to rise much more sharply than the theoretical results. Younger's calculation includes direct electron ejection from the 3p and 3s subshells only, but in this case excitation of 3s electrons to highly excited shells may lead to the formation of autoionizing configurations $[Ne]3s^1 3p^2 nl$ for $n \geqslant 8$, which are seen to contribute to the SI cross section.

3.1.2. Ar^{5+}. Ar^{5+} belongs to the aluminium isoelectronic sequence. The first threshold is observed at 74 $\pm$ 2 eV, which is 17 eV below the ground state ionization threshold. It is clear that the primary ion beam contains a weak but non-negligible population of the metastable excited configuration ($1s^2 2s^2 2p^6 3s 3p^2$) whose ionization thresholds corresponding to the spectroscopic terms (^{4}P, ^{2}D, ^{2}S and ^{2}P) are scattered between 68.4 and 78.6 eV. The uncertainty associated with the determination of the threshold does not allow the precise identification of

Table 2. Observed and calculated thresholds for different ionization processes involved in the present work. [Ne] stands for the $1s^2 2s^2 2p^6$ configuration. SI_{th}, EA_{th}, DI_{th} and IA_{th} are calculated ionization and excitation thresholds (from Bashkin and Stoner 1975 and Clementi and Roetti 1974). SI_{obs}, EA_{obs}, DI_{obs} and IA_{obs} are the observed ionization and excitation thresholds. *g* and *m* indicate the ground state and the metastable state, respectively.

Ion	State	SI_{th} (eV)	SI_{obs} (eV)	EA_{th} (eV)	EA_{obs} (eV)	DI_{th} (eV)	DI_{obs} (eV)	IA_{th} (eV)	IA_{obs} (eV)
Ar^{4+}	[Ne]$3s^2 3p^2\ ^3P$ (g)	3p: 75.02 3s: 87.52	75.1 ± 0.5 95 ± 5	2p: 249 2s: 324	—	(3p, 3p): 166.1	—	2p: 328 2s: 403	—
Ar^{5+}	[Ne]$3s3p^2\ ^2S$ (m)	$3p^*$: 68.4–78.6	74 ± 2	2p: 232 (m)	220 ± 10	—	—	2p: 329 2s: 404	325 ± 5 400 ± 10
	[Ne]$3s^2 3p\ ^2P$ (g)	3p: 91.0 3s: 105.2 3s: 112.2	87 ± 5 106 ± 2 132 ± 3	2p: 253 2s: 350	—	(3s, 3p): 215.3	215 ± 5	2p: 350 2s: 425	—
Ar^{6+}	[Ne]$3s3p\ ^3P$ (m)	3p: 110.3	108 ± 5	2p: 245	237 ± 3	(3s, 3p): 253.8	250 ± 5	2p: 359 2s: 431	355 ± 5
	[Ne]$3s^2\ ^1S$ (g)	3s: 124.3	—	2p: 259 2s: 334	257 ± 3	(3s, 3s): 267.8	—	2p: 373 2s: 445 1s: 3346	—
Ar^{7+}	[Ne]$3s^2S$ (g)	3s: 143.5 2p: 394.7	—	2p: 249 2s: 321	—	(3s, 2p): 566 (3s, 2s): 641 (2s, 2s): 996	635 ± 5	2p: 398 2s: 469 1s: 3361	3400 ± 100
Ar^{8+}	$1s^2 2s^2 2p^6\ ^1S$ (g)	2p: 422.5 2s: 497.4	426 ± 4	1s: 3218	3175 ± 175	(2p, 2p): 902 (2p, 2s): 968 (2s, 2s): 1043	930 ± 20	1s: 3402	3300 ± 100
Ar^{9+}	$1s^2 2s^2 2p^5\ ^2P$ (g)	2p: 479.7 2s: 545.4	496 ± 25	1s: 2980	—	(2p, 2p): 1020 (2p, 2s): 1075 (2s,2s): 1141	1120 ± 20	1s: 3479	3325 ± 150
Ar^{10+}	$1s^2 2s^2 2p^4\ ^3P$ (g)	2p: 540.0 2s: 595.3	565 ± 35	1s: 2999	—	(2p, 2p): 1159 (2s, 2s): 1266	1200 ± 100	1s: 3629	3350 ± 150
Ar^{11+}	$1s^2 2s^2 2p^3\ ^4S$ (g)	2p: 618.7 2s: 671.1	665 ± 35	1s: 3089	—	(2p, 2p): 1305 (2p, 2s): 1355	—	1s: 3719	3650 ± 50
Ar^{12+}	$1s^2 2s^2 2p^2\ ^3P$ (g)	2p: 685.8 2s: 736.7	—	1s: 3100	—	—	—	1s: 3814	—

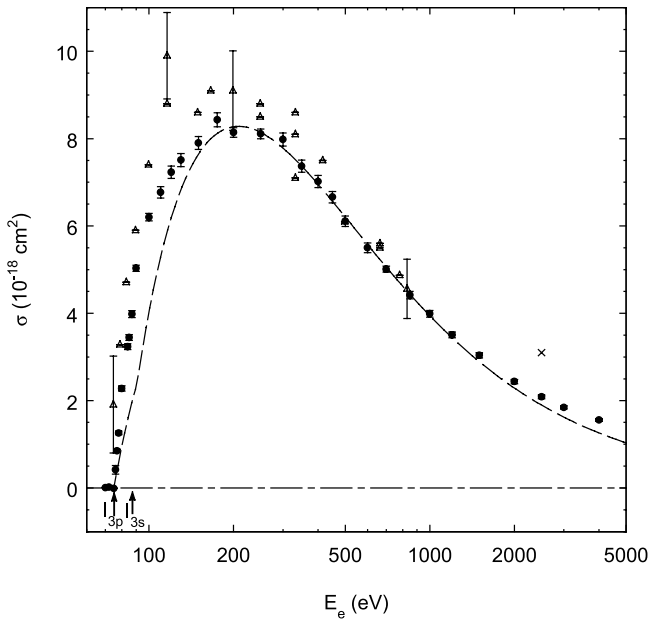

Figure 1. Absolute cross section for electron-impact SI of Ar^{4+}: •, present experimental results; △, Müller *et al* (1980); ×, Donets and Ovsyannikov (1981). The broken curve represents the DWBX of Younger (1981). I_{3p} and I_{3s} indicate the 3p and 3s subshell ionization thresholds.

the term, but it is likely that the ^{4}P state, which can only decay radiatively via spin inversion, has the longest lifetime of this group. The plateau observed just above the threshold is about 8% of the cross section maximum, indicating that the metastable state population should be of that order of magnitude. Results are shown in figure 2 together with those of Müller *et al* (1980) and Gregory *et al* (1985). Experimental data show good agreement above 400 eV only. Below that value, present data exhibit a non-monotonic behaviour, which was not observable in other experiments: clearly distinguishable steps are found around 87, 106, 132 and 220 eV. The lowest of them corresponds to the ground state ionization threshold which is expected to be at 91 eV. The second one (106 eV) corresponds to direct ejection of an electron from the 3s subshell. The peak observed between 132 and 200 eV was not previously observed for other charge states belonging to the same isoelectronic sequence: Si^+ (Djuric *et al* 1993), Fe^{13+} (Gregory *et al* 1987) and Ni^{15+} (Cherkani-Hassani *et al* 2001). The origin of this peak is still uncertain. Since the contamination of the Ar^{5+} primary beam by O^{2+} has no contribution to the true signal, the main difference observed in the present results is the significant metastable state population (see above), so that we may suppose that the peak should be attributed to a superposition of resonant capture processes followed by double autoionization (REDA) from the metastable states. Similarly to the preceding case ($q = 4$), above the ground state ionization threshold, the cross section is found to be much larger than the prediction for direct ionization (DWBX, Younger 1981), meaning that excitation of 3s electrons to highly excited shells also leads to the formation of autoionizing configurations $[Ne]3s^13p^1nl$ for $n \geqslant 8$. Above 220 eV, EA (from both the metastable and the ground states) to states belonging to the $1s^22s^22p^53s^23p^2$ configuration is seen to largely contribute to the ionization signal. The theoretical results of Younger (1981) and the semi-empirical Lotz formula (1968) take into account direct ionization from the ground state only, so they cannot reproduce any of the observed details.

Table 3. Electron impact SI cross sections (10^{-18} cm^2) for Ar^{q+} ($q = 4$–6). Uncertainties are one standard deviation on counting statistics.

E_e (eV)	Ar^{4+}	Ar^{5+}	Ar^{6+}	E_e (eV)	Ar^{4+}	Ar^{5+}	Ar^{6+}
70		0.008 ± 0.003		230		6.08 ± 0.16	2.27 ± 0.05
74		0.48 ± 0.39		235			2.29 ± 0.06
75	0.009 ± 0.002	0.60 ± 0.09		240			2.54 ± 0.06
76	0.42 ± 0.10			250	8.11 ± 0.11	6.29 ± 0.17	2.58 ± 0.06
77	0.85 ± 0.04			251			2.62 ± 0.07
78	1.26 ± 0.04			252			2.56 ± 0.06
80	2.28 ± 0.06	0.64 ± 0.08		253			2.71 ± 0.07
84	3.22 ± 0.07			255			2.67 ± 0.06
85	3.45 ± 0.07	0.65 ± 0.10		260			2.76 ± 0.06
87	3.98 ± 0.08			265			2.98 ± 0.07
90	5.03 ± 0.07	1.35 ± 0.06	0.016 ± 0.164	270		6.62 ± 0.16	3.27 ± 0.07
93		3.48 ± 0.14		280			3.45 ± 0.08
95		3.57 ± 0.11		300	7.98 ± 0.15	7.12 ± 0.17	3.69 ± 0.07
98		3.84 ± 0.24		330		6.99 ± 0.16	
100	6.20 ± 0.09	4.30 ± 0.15	0.070 ± 0.12	350	7.37 ± 0.14	6.49 ± 0.13	3.78 ± 0.08
101		4.81 ± 0.11		400	7.02 ± 0.14	5.97 ± 0.12	3.71 ± 0.07
103		4.82 ± 0.13	0.008 ± 0.005	450	6.66 ± 0.13		3.56 ± 0.07
105		4.93 ± 0.13		500	6.11 ± 0.12	5.52 ± 0.10	3.39 ± 0.07
108		5.27 ± 0.13		550			3.23 ± 0.07
110	6.77 ± 0.13	5.15 ± 0.18	0.21 ± 0.04	580			3.14 ± 0.07
113		5.31 ± 0.22		600	5.50 ± 0.10	5.04 ± 0.11	3.00 ± 0.06
120	7.23 ± 0.14	5.33 ± 0.19	0.39 ± 0.04	650			2.97 ± 0.06
125			0.54 ± 0.04	700	5.05 ± 0.07		2.87 ± 0.06
130	7.51 ± 0.15	5.30 ± 0.21	0.79 ± 0.06	800		4.12 ± 0.06	2.73 ± 0.06
135		6.05 ± 0.14		850	4.42 ± 0.09		
140		6.41 ± 0.11	1.04 ± 0.06	900		4.05 ± 0.05	
145		6.92 ± 0.08		1000	3.99 ± 0.08	3.48 ± 0.07	2.55 ± 0.05
147		6.99 ± 0.17		1200	3.51 ± 0.07	3.20 ± 0.06	2.27 ± 0.05
150	7.90 ± 0.15	7.93 ± 0.11	1.22 ± 0.05	1500	3.04 ± 0.06	2.82 ± 0.07	2.01 ± 0.04
155		7.09 ± 0.17		1700		2.56 ± 0.07	
160		6.97 ± 0.11	1.43 ± 0.06	1800			1.65 ± 0.04
170		6.82 ± 0.16		2000	2.44 ± 0.05	2.28 ± 0.07	1.68 ± 0.04
175	8.43 ± 0.16			2200		2.19 ± 0.07	
180		6.49 ± 0.10		2500	2.09 ± 0.04	2.00 ± 0.02	1.47 ± 0.04
190		6.41 ± 0.10		2800		1.80 ± 0.05	
200	8.14 ± 0.11	5.85 ± 0.13	1.84 ± 0.05	3000	1.85 ± 0.04	1.63 ± 0.05	1.36 ± 0.04
210		6.05 ± 0.13		3500		1.40 ± 0.05	
215			1.91 ± 0.06	4000	1.55 ± 0.03		1.18 ± 0.04
220		5.86 ± 0.08	2.21 ± 0.05				

3.1.3. Ar^{6+}. The data are shown in figure 3. The lowest observed threshold is located well below the ground state threshold at a position which indicates that a substantial fraction of ions formed in metastable states is present in the primary ion beam. This threshold corresponds to the [Ne]3s3p ^{3}P state which is expected to be located at 14.0 eV above the ground state ([Ne]3s^2 ^{1}S). Its lifetime is of the order of a few hundred milliseconds (Kaufman and Sugar 1986) which is much larger than the transit time (a few microseconds only) from the ion source to the collision region. No significant change of slope is observed at the expected ground state ionization threshold indicating that the metastable state is dominant.

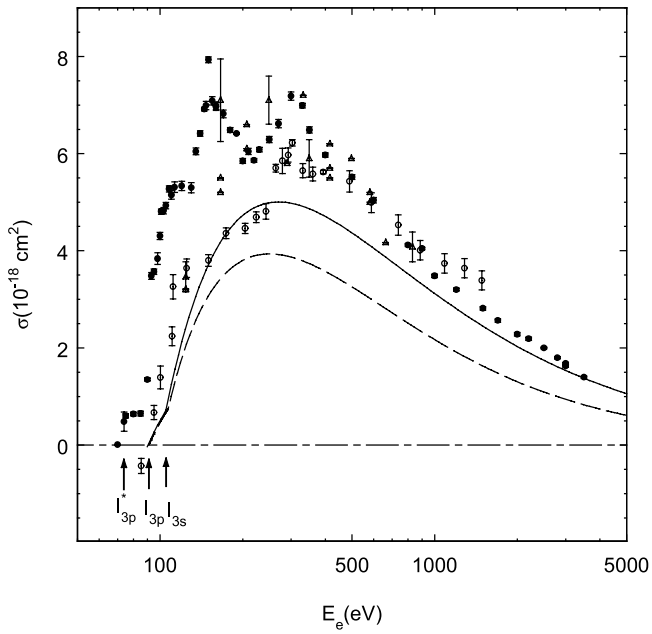

Figure 2. Absolute cross section for electron-impact SI of Ar^{5+}: •, present experimental results; (○) Gregory *et al* (1985) and (△) Müller *et al* (1980); broken curve represents DWBX (Younger 1981); full curve: Lotz formula (1968) for the ground state only. I^*_{3p}, I_{3p} and I_{3s} are the 3p and 3s subshell ionization thresholds for the metastable ([Ne]3s3p^2 ^{2}S) and for the ground state, respectively.

In figure 3, the results are compared to both sets of Oak Ridge Laboratory measurements (Howald *et al* 1986, Chung *et al* 1996). They do not agree with either, though their shape is similar in the whole common energy range. In particular, the low energy data show that the metastable content differs considerably between the three experiments. As a consequence, the contribution of excited ions to the ionization signal may vary considerably. The DWBX calculation performed by Younger (1981) underestimates the present data because it includes direct ionization from the ground state only. Above 220 eV, indirect processes contribute to about 50% of the signal. The processes are identified to be the excitation of 2p–*nl* and 2s–*nl* transition followed by autoionization, both from the metastable states and from the ground state. This conclusion results from the calculations of Pindzola *et al* (1986) which take into account direct ionization and EA from both configurations. The theoretical results underestimate the present one by some 15% around the maximum. The discrepancy could probably be removed by inclusion of REDA processes and by having a precise determination of the metastable content.

3.1.4. Ar^{q+} ($q = 8$–11). Experimental results for SI of Ar^{8+}, Ar^{10+} and Ar^{11+} are presented in figures 4 and 5. Previous experimental results are also shown: for $q = 8$ (Defrance *et al* 1987, Zhang *et al* 1991) and $q = 9$ (Rachafi *et al* 1987).

For Ar^{8+}, there is overall good agreement between various sets of experimental data except below the ground state ionization threshold where the presence of the $1s^22s^22p^53s(^3P)$ metastable state is not observed here, though it was clearly identified in experiments conducted at the Oak Ridge National Laboratory. It is worth mentioning that present data are not affected

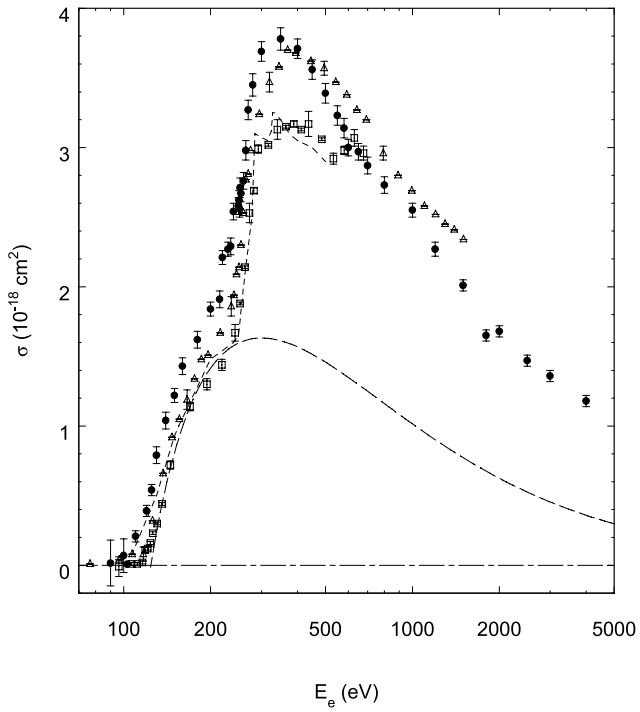

Figure 3. Absolute cross section for electron-impact SI of Ar^{6+}: •, present experimental results; △, Howald *et al* (1986); □, Chung *et al* (1996). The long-dashed curve represents the DWBX approximation (Younger 1981); the short-dashed curve represents the ACDW approximation (Pindzola *et al* 1986).

by background modulations as sometimes observed elsewhere. There is close agreement between the theoretical results (DWBX, Younger 1981, and ACDW, Pindzola *et al* 1986) and the prediction by means of the Lotz formula. All of them underestimate the cross section by some 10% around the maximum. The discrepancy is slightly larger in the low energy region. In this region, excitation to autoionizing states is also expected to play a role through the formation of $1s^2 2s2p^6 nl$ configurations ($n > 9$). This role should be weak as excitation cross section varies as n^{-3}. No other indirect ionization processes are observed.

For Ar^{9+}, the theoretical results of Laghdas *et al* (1995) exceed that of Rachafi *et al* (1987) by about 20%; they are based on the combination of the distorted-wave Born approximation and the *R*-matrix theory. For the three highest charge states ($q = 9$–11) a very good agreement is found with the prediction of the semi-empirical Lotz formula, taking into account the direct ionization of 2p and 2s electrons only. Again, no indirect process has been observed.

In figure 5, data are presented in a normalized Bethe plot: the product $\sigma I^2 (E/I)$ is plotted as a function of $\ln(E/I)$ where I is the ionization potential. When only direct SI processes are concerned, such a plot shows a quasi-linear dependence, whose slope is proportional to the number of active target electrons. This fact is clearly illustrated by the prediction of the Lotz formula and the experimental data precisely confirm that prediction.

3.2. Double ionization

Results are discussed in the three following sections for $q = 5$–6, 7 and 8–11, respectively, according to the respective active shells. As noted above, no theoretical result is currently

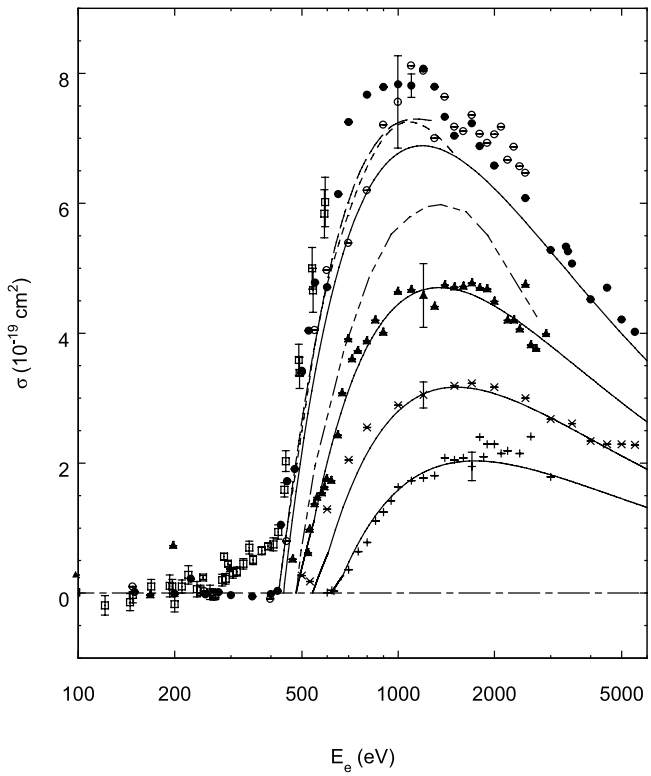

Figure 4. Absolute cross section for electron-impact SI of Ar^{q+} ($q = 8$–11): (•) Ar^{8+}, (×) Ar^{10+}, (+) Ar^{11+}, present results; (○) Ar^{8+}, Defrance *et al* (1987); (▲) Ar^{9+}, Rachafi *et al* (1987), (□) Ar^{8+}, Zhang *et al* (1991). The long-dashed curve represents the DWBX of Younger (1981) and the short-dashed curve represents the ACDW calculations of Pindzola *et al* (1986) for Ar^{8+}; the chain curve represents the *R*-matrix distorted-wave calculations of Laghdas *et al* (1995) for Ar^{9+} and the full curve represents the semi-empirical Lotz formula (Lotz 1968) for ground state ions.

available for any of these charge states. Fitting formulae (see, for instance, Bélenger *et al* (1997) or Fisher *et al* (1995)) provide a good tool for the prediction of DI cross sections but do not add any information to the discussion, so they will not be included here.

3.2.1. Ar^{q+}($q = 5$–6). Results for Ar^{5+} and Ar^{6+} are shown in figure 6 together with the experimental results obtained by Tinschert *et al* (1989). There is a good agreement between these sets of results in the whole common electron energy range. In spite of the very weak apparent cross section in the low energy region (about 2×10^{-20} and 4×10^{-21} cm^2 for Ar^{5+} and Ar^{6+}, respectively), the good precision of present data allows a detailed investigation of threshold effects. For Ar^{5+}, the observed threshold corresponds primarily to the ground state. Only a small contribution of the metastable state is expected because of its relatively small population, as indicated by the SI data. For Ar^{6+}, the current data clearly show the presence of an ionization signal below the lowest DI threshold. This confirms the presence of a long-lived metastable state in the primary Ar^{6+} ion beam which was observed in the corresponding SI cross-section measurement (see above). The DDI threshold for ground state ions is not observed, indicating that the corresponding contribution is less than the error bars due to the small ground state population.

Table 4. Electron impact SI cross sections (10^{-19} cm^2) for Ar^{q+} ($q = 8$, 10 and 11). Uncertainties are one standard deviation on counting statistics.

E_e (eV)	Ar^{8+}	Ar^{10+}	Ar^{11+}	E_e (eV)	Ar^{8+}	Ar^{10+}	Ar^{11+}
150	0.014 ± 0.120			1000	7.83 ± 0.18	2.89 ± 0.21	1.63 ± 0.16
200	-0.011 ± 0.390			1100	7.81 ± 0.18		1.73 ± 0.18
225	0.22 ± 0.09			1200	8.07 ± 0.18	3.05 ± 0.2	1.77 ± 0.14
250	-0.020 ± 0.006			1300	7.79 ± 0.16		1.81 ± 0.10
275	0.013 ± 0.078			1400	7.33 ± 0.18		2.08 ± 0.13
300	-0.033 ± 0.064			1500	7.04 ± 0.16	3.19 ± 0.19	2.05 ± 0.19
350	-0.053 ± 0.100			1600			2.08 ± 0.10
400	-0.017 ± 0.003			1700	7.23 ± 0.17	3.23 ± 0.2	1.95 ± 0.22
420	0.03 ± 0.03			1800	6.88 ± 0.17		2.4 ± 0.2
430	1.05 ± 0.12			1850			2.1 ± 0.15
450	1.72 ± 0.12			1900			2.29 ± 0.16
500	3.42 ± 0.18	0.27 ± 0.24		2000	6.58 ± 0.16	3.17 ± 0.14	2.29 ± 0.14
525	4.04 ± 0.20			2100			2.15 ± 0.2
530		0.18 ± 0.21		2200			2.19 ± 0.19
550	4.78 ± 0.16			2400			2.15 ± 0.27
600	4.71 ± 0.18	1.29 ± 0.24	0.008 ± 0.033	2500	6.08 ± 0.15	3.00 ± 0.13	
620			0.042 ± 0.21	2600			2.41 ± 0.33
630			0.03 ± 0.21	3000	5.28 ± 0.14	2.68 ± 0.12	1.79 ± 0.19
650	6.14 ± 0.24			3350	5.33 ± 0.14		
700	7.25 ± 0.18	2.05 ± 0.28	0.36 ± 0.24	3400	5.26 ± 0.14		
750			0.64 ± 0.12	3500	5.07 ± 0.14	2.61 ± 0.11	
800	7.67 ± 0.19	2.55 ± 0.29	0.78 ± 0.23	4000	4.52 ± 0.14	2.34 ± 0.11	
850			1.11 ± 0.32	4500	4.70 ± 0.10	2.29 ± 0.13	
900	7.79 ± 0.18		1.25 ± 0.16	5000	4.21 ± 0.14	2.29 ± 0.14	
950			1.42 ± 0.18	5500	4.02 ± 0.16	2.28 ± 0.18	

As expected, inner-shell ionization predominantly contributes to DI as autoionization follows with a branching ratio close to unity. Three different shells are in this favourable condition: the 2p, 2s and 1s shells. The cross sections exhibit a drastic change of slope in the energy range corresponding to 2p ionization. For both Ar^{5+} and for Ar^{6+}, the positions of these changes (325 $\pm$5 eV and 355 $\pm$ 5 eV) are well below the 2p ionization threshold (350 eV and 373 eV) for the ground state ions. For Ar^{5+}, other indirect processes are probably playing a role: resonant capture followed by triple auto-ionization or auto-triple ionization (RETA or REATI) and excitation followed by double autoionization or auto-double ionization (EDA or EADI). A similar shift was recently observed for multiply charged krypton ions (Khouilid *et al* 2001). For Ar^{6+}, the observed energy shift corresponds to the lowering of the indirect IA thresholds for ions formed in the excited states. The role of the 2s shell in the IA mechanism cannot be identified.

For a given charge state q, the DI cross section (σ_d^q) may be written as

$$\sigma_d^q = \sigma_{dd}^q + A_a \sigma_{ia}^q \tag{2}$$

where σ_{dd}^q and σ_{ia}^q describe DDI and inner-shell ionization, respectively. A_a is the branching ratio for autoionization, which is assumed to be equal to unity in the present discussion. σ_{ia}^q can be estimated by means of a semi-empirical formula (here the Lotz formula (Lotz 1968)). The corresponding results (curves in figure 6) are found to be in satisfactory agreement with the present results. In addition for Ar^{5+}, the small bump observed above 3 keV is probably due to K-shell ionization or excitation, followed by SI or DI, respectively. Finally, it is worth

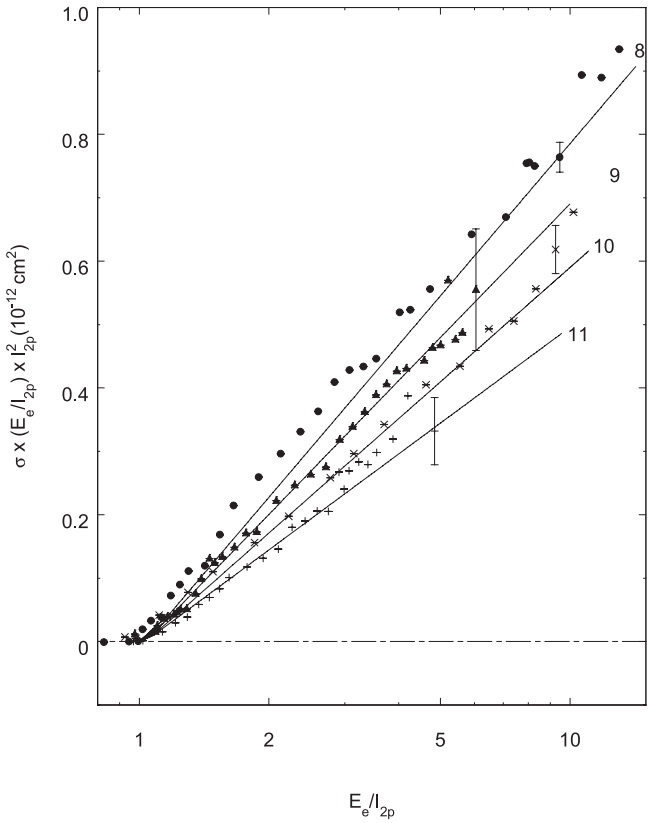

Figure 5. Bethe plot of present data for Ar^{q+} ($q = 8$–11). Symbols are identical to figure 4.

mentioning that σ_{dd}^{q} does not follow the classical Thomson scaling law which holds for SI. This is illustrated by comparing the ratio $\sigma_{dd}^{q}/\sigma_{d}^{q}$ along an isoelectronic sequence. This ratio is found to be 9% for Ar^{5+} while it was found to be only 3% for Ni^{15+} (Cherkani-Hassani *et al* 2001).

3.2.2. Ar^{q+}($q = 7$–11). These cross sections are located in a very low range (10^{-21}–10^{-20} cm^2) and, according to the very weak registered signals, the precision of present data is quite poor (as low as about 20% for $q = 11$), so a detailed analysis of these results is not possible. The results are shown in figures 7 and 8 for $q = 7$ and for $q = 8$–11, respectively.

For Ar^{7+}, the present results are found to be in satisfactory agreement with the former low-precision results, which were obtained previously in our laboratory (Rachafi *et al* 1991), but they are about a factor of ten lower than the cross sections obtained in the Giessen laboratory (Tinschert *et al* 1989) at two electron energies only (750 and 900 eV). This high result was possibly attributed to the presence of an autoionizing metastable state in the primary beam. No indication of such an effect was found in the present experiment. The dominant process is DDI, the indirect IA contribution of the K-shell not being visible. The observation of the lowest ionization threshold (635 ± 5 eV) confirms that the most weakly bound electron pair (3s, 2p) does not play any role in the DDI process: the first efficient electron pair is the (3s, 2s) one.

For $q = 8$–11, the observed position of DDI thresholds is not precise at all or even not observable ($q = 11$) and a threshold shift is clearly visible only for Ar^{9+}, leading to the same

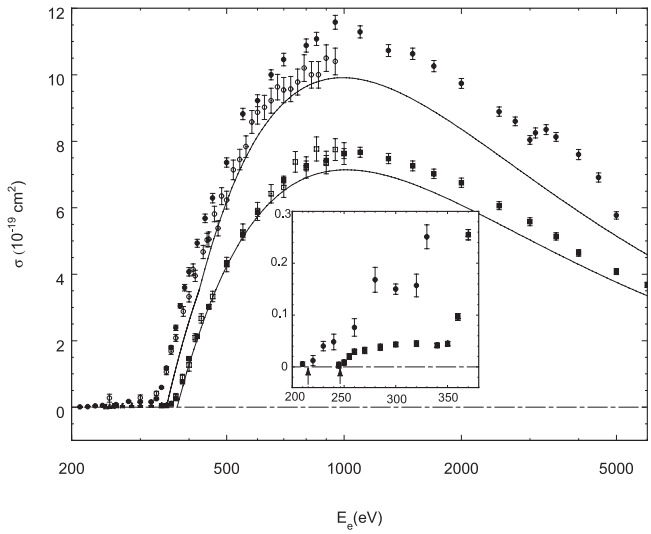

Figure 6. Absolute cross section for electron-impact DI of Ar^{5+} and Ar^{6+}: • and ■, present results; ○ and □, Tinschert *et al* (1989). The full curve represents the semi-empirical Lotz formula (1968) for the ground state only.

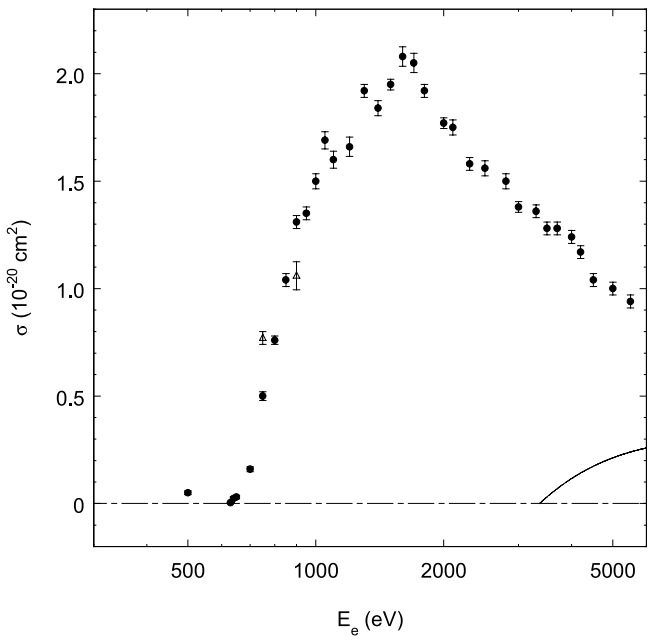

Figure 7. Absolute cross section for electron-impact DI of Ar^{7+}: •, present results, △, Tinschert *et al* (1989) ($\sigma/10$). The full curve represents the semi-empirical Lotz formula (1968) for K-shell ionization autoionization.

conclusion as for Ar^{7+}. The relative contribution of IA involving the K-shell is increasing drastically, according to the strong reduction of DDI along the isonuclear sequence. The IA contribution is presented by means of the Lotz formula for $q = 11$ only, for which DDI is found to be negligible. The branching ratio for the radiative decay of argon hollow ions has

Table 5. Electron impact DI cross sections (10^{-19} cm^2) for Ar^{q+} ($q = 5$ and 6). Uncertainties are one standard deviation on counting statistics.

E_e (eV)	Ar^{5+}	Ar^{6+}	E_e (eV)	Ar^{5+}	Ar^{6+}
210	0.0055 ± 0.004		500	7.36 ± 0.14	4.32 ± 0.09
214	-0.251 ± 0.008		550	8.82 ± 0.17	5.21 ± 0.11
220	0.012 ± 0.01		600	9.22 ± 0.18	5.86 ± 0.12
230	0.040 ± 0.009		650	10.00 ± 0.15	
240	0.048 ± 0.015		700	10.46 ± 0.19	6.81 ± 0.14
245		0.0034 ± 0.0059	800	10.88 ± 0.2	7.26 ± 0.15
250		0.008 ± 0.005	850	11.08 ± 0.2	
255		0.02 ± 0.01	900		7.42 ± 0.15
260	0.076 ± 0.017	0.029 ± 0.005	950	11.58 ± 0.21	
270		0.032 ± 0.006	1000		7.63 ± 0.15
280	0.17 ± 0.02		1100	11.29 ± 0.18	7.67 ± 0.15
300	0.15 ± 0.01	0.043 ± 0.005	1300	10.73 ± 0.18	7.26 ± 0.15
320	0.16 ± 0.02	0.045 ± 0.006	1500	10.63 ± 0.17	7.26 ± 0.15
330	0.25 ± 0.02		1700	10.26 ± 0.17	7.02 ± 0.14
340	0.59 ± 0.02	0.041 ± 0.005	2000	9.74 ± 0.15	6.75 ± 0.14
350	1.17 ± 0.04	0.045 ± 0.005	2500	8.89 ± 0.14	6.06 ± 0.12
360	1.79 ± 0.05	0.096 ± 0.007	2750	8.6 ± 0.13	
370	2.39 ± 0.08	0.26 ± 0.01	3000	8.04 ± 0.13	5.58 ± 0.12
380	3.05 ± 0.07		3100	8.25 ± 0.15	
385		0.76 ± 0.02	3300	8.35 ± 0.15	
390	3.60 ± 0.10		3500	8.13 ± 0.13	5.14 ± 0.11
400	4.07 ± 0.13	1.46 ± 0.04	4000	7.6 ± 0.15	4.64 ± 0.10
420	4.93 ± 0.12	2.13 ± 0.05	4500	6.91 ± 0.14	
440	5.68 ± 0.13		5000	5.77 ± 0.11	4.08 ± 0.09
450		3.02 ± 0.07	6000		3.68 ± 0.08
460	6.29 ± 0.14				

been seen to be not larger than a few per cent for $q > 8$ (Costa *et al* 2001). The agreement with experimental results may be considered good.

It is interesting to note the irregular evolution of σ_{dd}^q along this isonuclear sequence: surprisingly, in spite of the reduction of the number of active electrons, σ_{dd}^7 is found to be of the same order of magnitude as σ_{dd}^5 but much larger than σ_{dd}^6. These effects—as well as the lowering of the ratio σ_{dd}^q/σ_d^q mentioned above—are strongly related to correlation between target electrons, but, up to now, no precise quantitative arguments have been found to give a support to the present discussion.

4. Conclusions

Absolute cross sections are reported for electron impact ionization of multiply charged argon ions: SI ($q = 4$–6, 8–11) and DI ($q = 5$–11) ions, from threshold to about 6000 eV. The analysis of low energy data indicates the presence of ions formed in metastable states in the ion source: a weak population for Ar^{5+} and an important one for Ar^{6+}. These populations are seen to play a role both for SI and for DI.

For SI, direct processes are seen to be dominant, indirect EA processes are present only for charge states 4–6: in the threshold energy region only, for $q = 4$ and 5, due to excitation of high n autoionizing configurations; above the 2p–3p excitation threshold for $q = 5$ and 6. In

Table 6. Electron impact DI cross sections (10^{-20} cm^2 and 10^{-21} cm^2 for $q = 7$ and 8–11, respectively). Uncertainties are one standard deviation on counting statistics.

E_e (eV)	Ar^{7+}	Ar^{8+}	Ar^{9+}	Ar^{10+}	Ar^{11+}	E_e (eV)	Ar^{7+}	Ar^{8+}	Ar^{9+}	Ar^{10+}	Ar^{11+}
400	-0.014 ± 0.01					1900		4.45 ± 0.29			
500	0.05 ± 0.02					2000	1.77 ± 0.07	4.08 ± 0.26	2.19 ± 0.26	0.63 ± 0.18	-0.098 ± 0.1
600	-0.02 ± 0.02					2100	1.75 ± 0.06	4.37 ± 0.26			
630	0.004 ± 0.003					2200		4.32 ± 0.27			
640	0.02 ± 0.02					2250			2.10 ± 0.20		
650	0.03 ± 0.02					2300	1.58 ± 0.07	4.8 ± 0.24		0.74 ± 0.19	
700	0.16 ± 0.02					2400		4.27 ± 0.16			
750	0.50 ± 0.04					2500	1.56 ± 0.07	4.33 ± 0.17	2.21 ± 0.35	0.8 ± 0.18	0.12 ± 0.18
800	0.76 ± 0.04					2586			2.13 ± 0.26		
850	1.04 ± 0.06					2600		4.51 ± 0.24			
900	1.31 ± 0.06					2700		4.28 ± 0.25		0.95 ± 0.18	
908		0.01 ± 0.02				2800	1.50 ± 0.05	4.5 ± 0.3	2.03 ± 0.28		
910		0.02 ± 0.09				3000	1.38 ± 0.06	4.36 ± 0.25	2.0 ± 0.27	0.82 ± 0.18	0.28 ± 0.11
950	1.35 ± 0.06	0.18 ± 0.06				3200		4.29 ± 0.26	1.56 ± 0.18	0.52 ± 0.07	
960		0.27 ± 0.14				3300	1.36 ± 0.06				
1000	1.50 ± 0.07	0.48 ± 0.15	0.075 ± 0.073	0.04 ± 0.13		3400		3.83 ± 0.26			
1050	1.69 ± 0.08	1.24 ± 0.14	0.085 ± 0.21			3450			1.73 ± 0.22		
1100	1.60 ± 0.08	1.83 ± 0.2	-0.158 ± 0.18			3500		3.86 ± 0.28	1.55 ± 0.22	0.54 ± 0.18	-0.08 ± 0.31
1120			0.193 ± 0.11			3600		4.03 ± 0.28	1.68 ± 0.18		0.041 ± 0.22
1145				0.004 ± 0.12		3650					0.44 ± 0.16
1150			0.348 ± 0.19			3700	1.28 ± 0.06		1.74 ± 0.19	0.95 ± 0.11	
1200	1.66 ± 0.09	2.51 ± 0.23	0.57 ± 0.12			3800		4.47 ± 0.29	2.26 ± 0.20		0.352 ± 0.12
1250			1.07 ± 0.22		0.0014 ± 0.0003	3900					0.75 ± 0.18
1300	1.92 ± 0.06	2.93 ± 0.28		0.35 ± 0.16		4000	1.24 ± 0.06	4.61 ± 0.27	2.28 ± 0.27	1.23 ± 0.15	0.92 ± 0.28
1400	1.84 ± 0.07	2.98 ± 0.27	1.31 ± 0.31		-0.23 ± 0.08	4200	1.17 ± 0.06		2.46 ± 0.24		
1450		3.34 ± 0.23				4250					1.21 ± 0.13
1500	1.95 ± 0.05	3.81 ± 0.27	1.55 ± 0.21	0.54 ± 0.14		4500	1.04 ± 0.06	4.32 ± 0.29	2.52 ± 0.20	1.41 ± 0.17	1.40 ± 0.15
1600	2.08 ± 0.09	3.77 ± 0.29				4750					1.79 ± 0.33
1649			1.73 ± 0.26			5000	1.00 ± 0.06	4.07 ± 0.27	2.70 ± 0.31	1.64 ± 0.18	1.77 ± 0.23
1700	2.05 ± 0.06	4.23 ± 0.27		0.55 ± 0.17	-0.038 ± 0.043	5250					1.71 ± 0.25
1800	1.92 ± 0.05	4.59 ± 0.32	2.13 ± 0.23			5500	0.94 ± 0.06	4.15 ± 0.31	2.72 ± 0.34	2.23 ± 0.21	1.72 ± 0.25

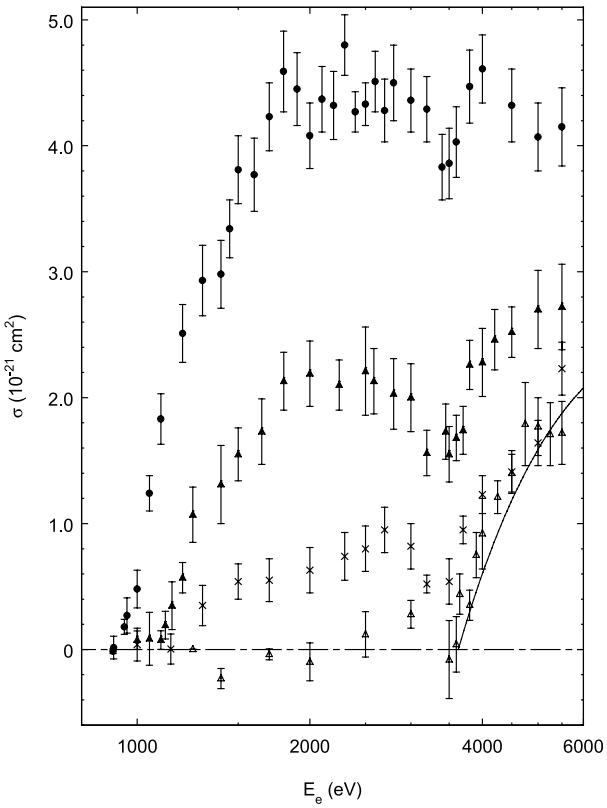

Figure 8. Absolute cross section for electron-impact DI of Ar^{q+} ($q = 8$–11). (•) Ar^{8+}, (▲) Ar^{9+}, (×) Ar^{10+}, (△) Ar^{11+}, present results. The full curve represents the semi-empirical Lotz formula (1968) for K-shell ionization autoionization (Ar^{11+} only).

addition, a superposition of resonant mechanisms seems to be the source of the peak observed for $q = 5$ between 132 and 200 eV.

For Ar^{5+} and Ar^{6+}, DI is seen to be dominated by IA involving the L shell. For higher charges, DDI is found to decrease drastically along the isonuclear sequence, leaving IA from the K-shell the one and only visible process for the highest charge state ($q = 11$). The semi-empirical Lotz formula (1968) offered a reasonable prediction of this process.

Acknowledgments

Most of the present results were part of the PhD thesis of one of us, Zhang Hui, who passed away after a very long illness without being able to present it. His co-workers are definitively indebted to him for his major contribution to this work. This paper is published in honour of his memory.

References

Bashkin S and Stoner J 1975 *Atomic Energy Levels and Grotrian Diagrams* vol 2 (Amsterdam: North-Holland) (1978 addendum)

Barué C, Biri S, Cherkani-Hassani S, Gealens M, Loiselet M and Ryckewaerst G 1989 *Rev. Sci. Instrum.* **69** (2) 764

Bélenger C, Defrance P, Salzborn E, Shevelko V P, Tawara H and Uskov D B 1997 *J. Phys. B: At. Mol. Opt. Phys.* **30** 2667
Bliman S, Bonnefoy M, Bonnet J J, Dousson S, Fleury A, Hitz D and Jacquot B 1983 *Phys. Scr.* T **3** 63
Cherkani-Hassani S, Khouilid M and Defrance P 2001 *Phys. Scr.* T **92** 287
Chung Y S *et al* 1996 Oak Ridge National Laboratory, unpublished data
Clementi E and Roetti C 1974 *At. Data Nucl. Data Tables* **14** 177
Costa A M, Martins M C, Parente F, Santos J P and Indelicato P 2001 *At. Data Nucl. Data Tables* **79** 223
Crandall D H, Phaneuf R A and Gregory D C 1979 *Electron Impact Ionisation of Multicharged Ions, ORNL Report* TM-7020
Defrance P, Brouillard F, Claeys W and Van Wassenhove G 1981 *J. Phys. B: At. Mol. Phys.* **14** 103
Defrance P, Kereselidze T M, Machavariani Z S and Noselidze I L 2000 *J. Phys. B: At. Mol. Opt. Phys.* **33** 4323
Defrance P, Rachafi S, Jureta J, Meyer F W and Chantrenne S 1987 *Nucl. Instrum. Methods* B **23** 265
Deutsch H, Becker K, Gstir B and Märk T D 2002 *Int. J. Mass Spectrosc.* **213** 5
Djuric N, Bell E W, Guo X Q, Dunn G H, Phaneuf R A, Bannister M E, Pindzola M S and Griffin D C 1993 *Phys. Rev.* A **47** 4786
Donets E D and Ovsyannikov V P 1981 *Sov. Phys.–JETP* **53** 466
Duponchelle M, Zhang H, Oualim E M, Bélenger C and Defrance P 1995 *Nucl. Instrum. Methods* A **364** 159
Fisher V, Ralchenko Y, Goldgirsh A, Fisher D and Maron Y 1995 *J. Phys. B: At. Mol. Opt. Phys.* **28** 3027
Gregory D C, Crandall D H, Phaneuf R A, Howald A M, Dunn G H, Falk R A, Mueller D W and Morgan T J 1985 *Electron Impact Ionisation of Multicharged Ions at ORNL: 1980–1984* ORNL/TM-9501
Gregory D C, Wang L J, Meyer F W and Rinn K 1987 *Phys. Rev.* A **35** 3256
Howald A M, Gregory D C, Meyer F W, Phaneuf R A, Müller A, Djuric N and Dunn G H 1986 *Phys. Rev.* A **33** 3779
Janev R K 1993 *Summary Report of the IAEA Technical Committee Meeting on Atomic and Molecular Data For Fusion Reactor Technology Agency (Vienna)*
Kaufman V and Sugar J 1986 *J. Phys. Chem. Ref. Data* **15** 321
Khouilid M, Cherkani-Hassani S, Adimi N, Rachafi S and Defrance P 2001 *J. Phys. B: At. Mol. Opt. Phys.* **34** 3239
Laghdas K, Reid R H G, Joachain C J and Burke P G 1995 *J. Phys. B: At. Mol. Opt. Phys.* **28** 4811
Lotz W 1968 *Z. Phys.* **216** 241
Müller A, Salzborn E, Frodl R, Becker R, Klein H and Winter H 1980 *J. Phys. B: At. Mol. Phys.* **13** 1877
Pindzola M S, Griffin D C and Bottcher C 1986 *Phys. Rev.* A **33** 3787
Pindzola M S, Griffin D C and Bottcher C 1990 *Phys. Rev.* A **41** 1375
Rachafi S, Jureta J and Defrance P 1987 *Proc. 15th Int. Conf. on the Physics of Electronic and Atomic Collisions (Brighton)* p 378 (book of contributed papers)
Rachafi S, Belic D S, Duponchelle M, Jureta J, Zambra M, Zhang H and Defrance P 1991 *J. Phys. B: At. Mol. Opt. Phys.* **24** 1037
Tinschert K, Müller A, Phaneuf R A, Hofmann G and Salzborn E 1989 *J. Phys. B: At. Mol. Opt. Phys.* **22** 1241
Younger S M 1981 *Atomic Data for Fusion* Oak Ridge National Laboratory **7** 190
Zhang Y, Reddy C B, Smith R S, Golden D E, Mueller D W and Gregory D C 1991 *Phys. Rev.* A **44** 4368